The Free Surface of Thin Diblock Copolymer Films: Experimental and Theoretical Investigations on the Formation and Growth of Surface Relief Structures

P. C. M. Grim,[†] I. A. Nyrkova,[‡] A. N. Semenov,[‡] G. ten Brinke,[†] and G. Hadziioannou*,[†]

Department of Polymer Chemistry, University of Groningen, Nijenborgh 4, 9747 AG Groningen, The Netherlands, and Physics Department, Moscow State University, Moscow 117234, Russia

Received March 7, 1995; Revised Manuscript Received July 28, 1995[⊗]

ABSTRACT: We have investigated both experimentally and theoretically the formation and subsequent growth of surface relief structures on thin diblock copolymer films. The surface pattern appearing upon annealing is characterized by the average domain radius R. Using atomic force microscopy, we have obtained time-dependent topographs from which the critical exponent α in the growth law $R \propto t^{\alpha}$ has been determined. The values are significantly lower than the ones usually predicted for α in such films. We have discussed theoretically both the nucleation and formation stage of the process in detail, also considering the ideal situation (all domains belong to the same lamellar layer, and no additional defects are present). In particular the dependence of the growth law on the surface fraction Φ occupied by domains was addressed. For the ideal situation three main values of the exponent α were predicted: $^1/_4$, 1, and $^1/_3$. However, we show that several factors can be responsible for a decrease in the apparent exponent α, such as line defects, semi-islands, and the multilayer character of the domain pattern. A crucial role of the line defects, especially for small values of Φ, is predicted. Theoretical results are in qualitative agreement with the experimental data.

I. Introduction

The phenomena of microphase separation in block copolymers have made them materials of great technological importance. Depending on the ratio of the block lengths, the well-known family of morphologies of microstructures in the bulk can emerge.[1] The size of the microdomains is determined by the structure of the blocks (primarily by the lengths of the constituent blocks). The macroscopic properties of the block copolymer (e.g. structural, electrical, and/or optical) can be controlled during polymer synthesis. Block copolymers are, e.g., very useful as surface modifying agents in polymer blends, for colloidal stabilization, in high-impact plastics, and as thin-film adhesives. In all cases, the fundamental understanding of block copolymers at surfaces and interfaces is of crucial importance.

For surface modification, block copolymers possessing lamellar ordering are of great technological importance, because in the ideal case they give rise to a surface coverage shown in Figure 1a. In general, when a thin film of nearly symmetric diblock copolymer is deposited onto a flat substrate, the difference in surface energy of the two blocks leads (upon annealing) to an orientation of the lamellae parallel to the substrate and hence to an accompanying quantization in the film thickness in the ordered state. The local thickness of the film satisfies the equation $d_n = nH$ or $d_n = (n + 1/2)H$, depending on whether like or unlike blocks are present at the polymer−air and polymer−substrate interface (H is the lamellar periodicity of the system). In reality, after sample preparation, the initial thickness d of the film is always such that $d_n \leq d \leq d_{n+1}$ for some value of n. In the ordered state, the free surface will therefore consist of areas with thickness d_n and of areas with thickness d_{n+1}. These are the well-known relief structures (islands or holes) which appear on the top surface upon annealing of the thin block copolymer film above the glass transition temperature of both blocks (see Figure 1b,c). If $d_n < d < (d_n + d_{n+1})/2$, the relief structures are elevations (islands), and if $(d_n + d_{n+1})/2 < d < d_{n+1}$, they are depressions (holes). With increasing annealing time the pattern of relief structures

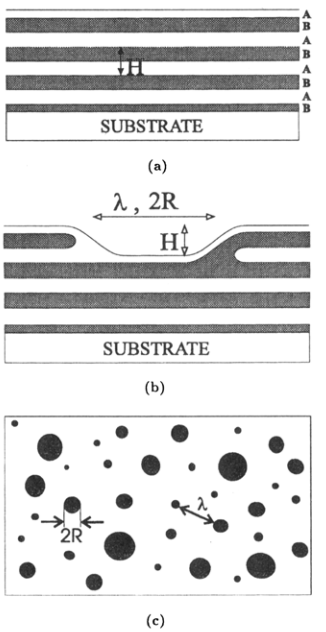

Figure 1. (a) Lamellar ordering of a thin block copolymer film at a surface. (b) Schematical cross section of the relief structures in a thin diblock copolymer film. White and gray regions correspond to parts of the film occupied by A and B blocks, respectively. In practice, the edge angle is 6−12°, which is much smaller than indicated in the schematic drawing. (c) Top view of the pattern of surface relief structures. The pattern is characterized by a domain radius R and an interdomain distance λ.

[†] University of Groningen.
[‡] Moscow State University.
[⊗] Abstract published in *Advance ACS Abstracts,* September 15, 1995.

0024-9297/95/2228-7501$09.00/0

evolves toward a decrease of the total length of the domain boundaries; hence the typical size of the domains (islands or holes) increases. The driving force for this process is the edge defect line tension energy connected with the border lines of the domains.

Such "quenching" kinetics of relief structures at free surfaces of thin block copolymer films has received widespread attention in recent years and a number of experimental studies have been devoted to the formation and subsequent growth of the relief structures employing techniques like optical microscopy,[2] reflectivity (X-ray,[3] neutron[4]), secondary ion mass spectrometry,[5] and atomic force microscopy.[6] Recently, transmission electron microscopy experiments have been performed,[7] showing that at the domain edges of holes and step edges of terraces, the lamellar directors are aligned parallel to the plane of the substrate. A transition in the lamellar alignment within steps is predicted from homogeneous (director || substrate) to homeotropic (director ⊥ substrate), when the film thickness is increased. This transition is supposed to occur above a certain number of lamellar layers between 3 and 8.

In addition to the technical importance of the process of lamellar ordering on surfaces, this process of surface pattern growth can be used as a convenient model for studying the kinetics of phase separation in two dimensions.[8] The characteristic depth H of the relief structures is on the order of hundreds of angstroms (it coincides with the periodicity of the lamellar structure), and the relief pattern growth process can be observed at time scales from several minutes to several tens of hours, the characteristic surface length scale (the radii of the islands (holes), R, or the interdomain distance, λ; see Figure 1b,c) being of micrometer size scale (0.1–50 μm). This allows the direct observation of shape, size, and growth behavior of the domain structures using techniques like atomic force microscopy[6] and optical interference microscopy.[2] Three characteristic surface processes are observed by which the growth of the relief domains evolves: individual growth, coalescence, and dissolution of domains. It is the dependence of the characteristic dimension of the domain structures, R (or λ) versus quenching time t and the corresponding critical exponent α ($R \propto t^{\alpha}$), that is usually reported.

Due to the fact that the growth process of relief structures in block copolymer films resembles ordinary first-order transitions, mostly an oversimplified description of this phenomenon was used for the theoretical models, in which the molecular structure of the block-copolymer layers was not taken into account. As a result, in most of these theoretical papers the classical Lifshitz–Slyozov[9] result ($\alpha = 1/3$) has been achieved.[10,11] Sometimes, more sophisticated models were used,[12,13] but still the system was treated as an ordinary two-phase system, and the real structure of the block-copolymer film was not taken into account. As a result, the strong discrepancy between experimental data and theoretical predictions was not understood up to date. For example, experimental data often show that the value of the exponent α can change with the time scale of the annealing process and also α is dependent on the fraction Φ ($\equiv \pi R^2/\lambda^2$) of the surface area occupied by islands (holes).[8] We stress that in the formation and growth of the surface relief structures several mechanisms are competing, and hence various parameters of the block copolymer melt control this process. The first attempt to give a molecular description of the domain growth process was made only recently.[14] In this paper the relief structure evolution was considered for an ideal (defectless) thin diblock copolymer film. All the islands (holes) were supposed to be in the same top layer of the film, and the following three fundamental mechanisms were proposed and analyzed: diffusion of entire domains, tunneling of polymer molecules through the foreign layer, and two-dimensional pressure relaxation. The latter mechanism was shown to be the most important one for sufficiently long annealing times. However, it leads again to a growth exponent of $\alpha = 1/3$ (Lifshitz–Slyozov result), while in most experiments a lower growth exponent is observed for this kind of system.[8,15]

The present paper is aimed at investigating these problems in more detail. First, we present an experimental study concerning the development of the domain radius R with time using atomic force microscopy. Especially the dependence of the growth exponent α on the concentration of the domains on the surface, Φ, is investigated. In the Theoretical Part, we propose a possible explanation for the difference between the experimental and theoretical values for the growth exponent α. We pay attention to the possibility that not all domains belong to the same layer as well as to the role of defects (dislocations) in the lamellar structure. A comparison with experimental data leads to the conclusion that the defects play a crucial role in the relief structure growth process in the block-copolymer films under consideration, leading to a decrease in the observed growth exponent. Also, we give an estimate for the possible defect structure density and its influence on the apparent values for the growth exponent α.

II. Experimental Part

A. Sample Preparation. The polymer that has been used in this study is a 60k/68k polystyrene/poly(2-vinylpyridine) (PS/P2VP) diblock copolymer. It was prepared by anionic polymerization in THF solution at −78 °C under ultrahigh purity argon.[16] The polymer was characterized by gel permeation chromatography and elemental analysis. The PS and P2VP block molecular weights were determined to be 60k and 68k, respectively, with a dispersion in the molecular weight of 1.21. For the preparation of the thin films, the polymer was dissolved in toluene (concentration 0.03 g/mL). The silicon substrates onto which the polymer was spin coated were rinsed with pure toluene just prior to the spin-coating procedure. The spin-coating procedure was as follows. A few drops of filtered polymer solution were put on the silicon substrate so that the solution covered the entire substrate. Then the substrate was rotated for 45 s at the desired spinning speed (between 2000 and 3000 rpm). Most of the solution is swept aside and only a thin layer remains, out of which the solvent evaporates very quickly. This procedure yields homogeneous, flat films with a thickness d of 2000–3000 Å, roughly corresponding to 4–8 layers of the lamellar structure (in the ordered state). The thickness d of the film can be controlled by varying the concentration of the solution and the spinning speed. An estimate can be obtained from the interference colors in the optical microscope. For the given system, the P2VP block possesses an affinity for the silicon–polymer interface and the PS block has an affinity for the free surface. The possible values for the thickness in the ordered state are therefore $(n + 1/2)H$. The lamellar periodicity H (see Figure 1) is 430 ± 20 Å. This has been determined from transmission electron microscopy measurements performed on bulk samples and also from the height of the domains in the AFM topography images.

B. Atomic Force Microscopy. The thin polymer films were investigated by means of atomic force microscopy[17] (AFM), which has proven to be a very successful technique in surface science owing to its ability to visualize solid surfaces from the micrometer level down to the atomic scale. It can be applied to conducting, nonconducting, organic, and inorganic

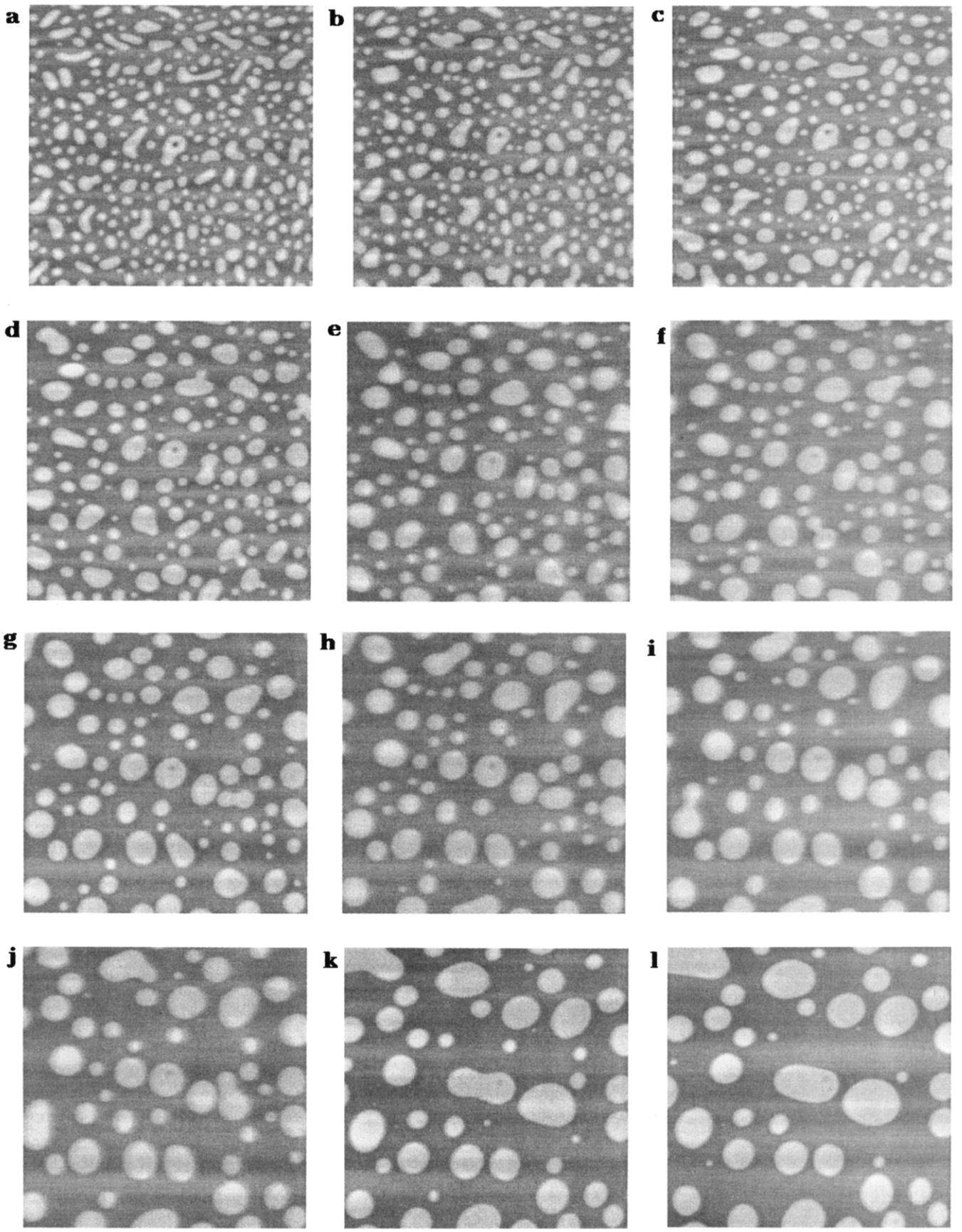

Figure 2. AFM topographs of the evolution process of the surface relief structures obtained at various annealing times on identical surface areas: (a) 132 s, (b) 198 s, (c) 344 s, (d) 590 s, (e) 836 s, (f) 1202 s, (g) 1622 s, (h) 2168 s, (i) 2834 s, (j) 3800 s, (k) 6332 s, (l) 8864 s. Each image covers an area of 35 × 35 μm^2.

materials in various environments. A review of organic materials investigated by AFM is given in ref 18. Not only sample topography can be studied, but also friction, adhesion, magnetic, and electrostatic forces can be probed. In atomic force microscopy, a sample is scanned (using piezoelectric elements) underneath a sharp tip which is in repulsive contact with the sample surface. This sharp tip is connected to a soft cantilever spring whose deflection is monitored, usually by

means of the laser beam deflection method. In this way, variations in the local polymer surface structure can be visualized.

All the measurements were carried out using a commercial system (Park Scientific Instruments). The AFM images were recorded in the constant force mode in air, using standard Si_3N_4 cantilevers (force constant of 0.1 N/m). The applied force was approximately 10 nN. No damage was observed on the sample surface even after repeated scanning of the same surface area. This standard AFM setup has been complemented with a small hot stage and a vacuum chamber. In this way, it is possible to anneal the samples in vacuum inside the AFM, so that exactly the same sample area can be relocated after annealing. The hot stage, consisting of a copper disk, is sandwiched between the sample holder and the sample itself. A temperature controller was designed to adjust and control the temperature of the sample. The homemade vacuum chamber consists of a base plate on which the AFM can be placed and a glass cover. On the base plate are mounted connectors (for AFM and hot-stage operation). Also the vacuum pump is connected to this base plate. During the annealing process, the AFM was put in the vacuum chamber to avoid degradation of the polymer film. In order to obtain the time-dependent relief structure measurements, the samples were annealed in a stepwise manner. Prior to each annealing step, the AFM tip was retracted from the sample surface. The AFM was put in the vacuum chamber and the sample was heated to the desired annealing temperature (180 °C) for a certain period of time (the glass transition for both PS and P2VP is slightly above 100 °C). The sample was allowed to cool to room temperature before the tip was again lowered and the next image recorded. The time-dependent ordering process of the top surface of the thin polymer film could thus be followed at a local scale.

C. Relief Structure Growth Data. After spin coating, the sample surfaces are very flat (typical roughness on the order of 1 nm). As annealing time increases, this flat top surface vanishes rather quickly as a result of the formation of domain structures (islands or holes). This happens on a time scale of a few minutes. This specific surface pattern subsequently grows with increasing annealing time. As an example of the evolution of the top surface, some stages in the growth process of one particular sample are shown in Figure 2. The three mechanisms by which the surface structure develops with time, growth of individual islands, coalescence of neighboring islands, and the dissolution of islands, are evidently visible from subsequent AFM topographs.

The AFM images recorded at various stages of the coarsening process were analyzed using a Kontron image analysis station. Individual and average island (or hole) areas as well as the surface coverage Φ of the islands (holes) were determined as a function of time. The results of this analysis are shown in Figure 3. In Figure 3a the surface coverage Φ of the islands of one of the samples is presented as a function of annealing time. After an initial increase during the formation stage, the fraction of the top surface covered with islands becomes constant (coalescence stage). Small variations in this constant value can be due to small drift during AFM scanning or variations in domain boundary determination during the image analysis procedure. In general, in AFM, the surface profile is convoluted with the shape of the tip. For example, a sharp step on a surface will be imaged as a much more gradual transition from the lower to the higher level. The measured profile strongly depends on the shape of the tip and especially on the tip end radius, which is approximately 30–40 nm. In our case, the domain boundary profiles of the relief structures are not exactly sharp steps. The transition from the lower to the higher level (step height H) occurs within a region of 400–500 nm. This is too large for any tip-shape convolution effects to influence the observed AFM edge profiles,[19] but the relative error in the determination of the domain area can be quite substantial. An error of 10% of the total width of the edge profile is reasonable for the determination of the domain areas. For small domains ($R \leq 1\ \mu m$), this results in a relative error in the domain area of 10% or more. For larger domains, this error decreases inversely

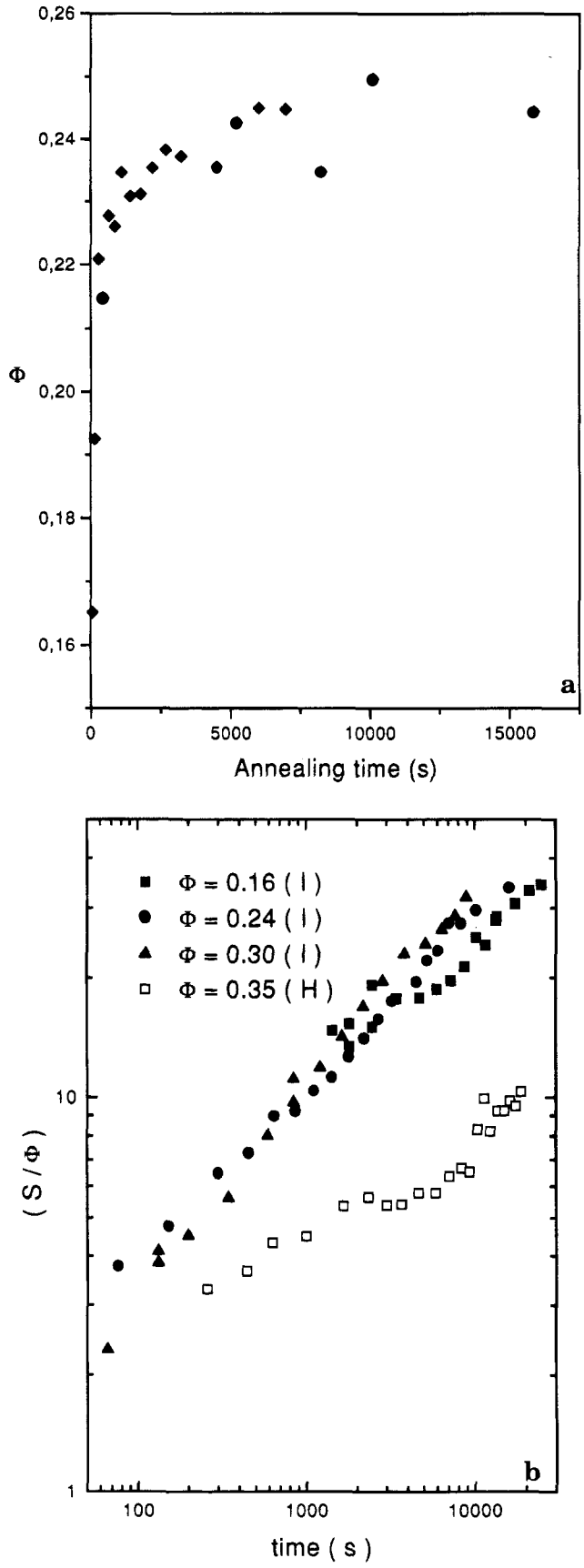

Figure 3. Analysis of the AFM topographs: (a) surface fraction Φ occupied by islands as a function of annealing time for one particular sample; (b) double logarithmic plot of (S/Φ) as a function of annealing time.

proportional with the domain radius. Domains which are not entirely within the field of view of the AFM scan were disregarded in the analysis as far as the average radius is

Table 1. Growth Exponents α for Various Values of the Surface Fraction Φ Occupied by Domains

islands (I)/ holes (H)	Φ	α	islands (I)/ holes (H)	Φ	α
I	0.16	0.15	I	0.30	0.26
I	0.24	0.21	H	0.35	0.12

concerned. Of course, they are taken into account for the determination of the surface coverage Φ. Figure 3b shows the mean interdomain distance time dependence for various island/hole structures, $\lambda(t)$. This distance was determined via the ratio of the number-averaged domain area $S(=\pi R^2)$ and the surface coverage of the domains Φ:

$$\lambda^2 \equiv \frac{S}{\Phi} = \frac{\pi R^2}{\Phi} \tag{1}$$

Fitting this to $S = \pi R^2 \sim t^{2\alpha}$ yields a value for the growth exponent α. Table 1 gives an overview of the growth exponents obtained for the different diblock copolymer samples. [The measurements acquired during the formation stage have not been taken into account for the determination of the growth exponent α. In principle, it is also possible to fit the data according to the expression $R^{\alpha'} \sim R_0 + kt$. This has been done and yields growth exponents α′ which are equal to or less than α]. A few striking results can be observed. Firstly, the growth exponent increases with the surface coverage of islands. Secondly, the growth exponents are, in many cases, smaller than 1/4. However, for defectless films, in accordance with the molecular model analysis presented in the literature,[14] the complete list of possible exponents is {1/4, 1/3, 1/2, 1}. One should find an explanation for this discrepancy. This will be the aim of the forthcoming theoretical part.

III. Theoretical Part

A. Stages and Problems Connected with the Relief Domain Growth Process on the Top Surface of Thin Block Copolymer Films. After spin coating, when the process of solvent evaporation has terminated, the structure of the film is practically disordered. Lamellae do already exist although they are not oriented with respect to the substrate. Some period of annealing at temperatures higher than the glass transition temperature (which is much higher than the ambient temperature at which the spin coating takes place) is needed for the orientation of the lamellae and the appearance of the domain structures. In the plots of the surface area fraction Φ occupied by domains versus annealing time t, two stages of the domain evolution process can be clearly distinguished (cf. Figure 3a). During the first stage the area fraction of domains Φ increases with time, and during the second stage Φ is practically constant. In accordance with the traditional classification for spinodal decomposition processes[20] these stages are the so-called nucleation (or formation) and coalescence (or growth) stages, respectively. They will be considered separately in more detail below.

The main process during the first stage is the formation of *critical* domains. After the spin-coating process, the thickness of the film is not equal to an equilibrium value (half-integer multiple of the equilibrium layer thickness H), and therefore some elastic energy is stored in the disturbed film. This elastic energy can relax through the formation of domain structures, so that now the local thickness of the film in each point coincides with a half-integer number of layers. This relaxation process is connected with the formation of dislocations (broken layers), which requires a certain amount of edge defect dislocation energy. As this dislocation energy is determined by the length of the defect, and the elastic energy which could relax is proportional to the area of the part of the film where the relaxation takes place, only rather large domains can be formed during this process. In connection with this two questions immediately arise:

1. What is the typical dimension of the islands (holes) appearing during this process?
2. What is the depth of the dislocations? (In which layer of the film are the domains formed?) These questions are the subjects of sections III.C.1. and III.C.2. below.

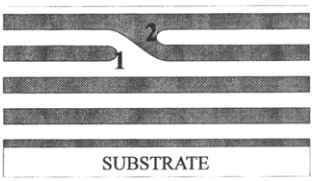

Figure 4. Ordinary defect in the lamellar structure. This defect is localized and not expected to diffuse as a whole.

Simultaneously with the formation of islands (holes), ordinary *defects* can also appear. A typical defect is shown in Figure 4. The thickness of the film does not change at the position of such a defect; so from a top view it is invisible. However, the layer structure is broken at this point: there are two edge disclinations at almost the same point of the film (marked by numbers "1" and "2" in Figure 4). As a result, additional borders appear in these layers which can be the edges of some islands or holes (cf. Figures 1b and 4). These defects can break the coherence of corresponding layers; so they strongly affect the kinetics of domain growth. Therefore, the density of such defects inside the film is of primary importance, and we will discuss the factors which can influence this defect density in section III.C.3.

The second stage of the spinodal decomposition process is the *coalescence* stage in which the domain structures, primarily formed during the first stage, relax toward an increase of the typical domain size. The elastic energy of the film has already completely relaxed by the formation of domains, so that locally the thickness of the film has attained an equilibrium value, i.e. nH or $(n + 1/2)H$ depending on the surface tensions of the upper and lower boundaries of the film. Due to the condition of incompressibility of the block copolymer melt, the total area of domains is constant: Φ = const. The driving force for the coalescence process is the minimization of the total energy associated with the edge dislocations. Having considered the molecular structure of the block copolymer films, we proposed *three main mechanisms* for the relief structure growth in a *defectless* film.[14] In section III.D.1 below we will recall the main ideas of this classification of relaxation processes in a defectless film with a one-layer domain structure, and we will present estimations for the corresponding characteristic times.

However, it is clear that the formation processes during the first stage of spinodal decomposition should lead to a more complicated structure of the film. One should consider the following possibilities: (1) Not all the dislocations necessarily belong to the same layer; hence in the evolution of the relief pattern, several relaxation processes in different layers can interfere. (2) More complicated structures (others than ordinary islands or holes) can appear in the film. (3) The defects (e.g. of the type shown in Figure 4) prevent flow relaxation in broken layers; hence the relaxation processes are slowed down tremendously. These possibilities will be investigated in sections III.D.2 and III.D.3

below. The theory in this paper is restricted to the homeotropic case (lamellar director perpendicular to the plane of the substrate) because we believe this situation is applicable to the experimental situation described in this paper.

B. Model. In the forthcoming sections we will use the following theoretical model. The film is supposed to be made of symmetric diblock copolymer AB. Each block consists of N monomer links, a being the link length, ζ being the friction coefficient of the link, and $v = a^3$ being the link volume. We suppose that the incompatibility of the blocks is high enough, $\chi N > 5$ (where $\chi = \chi_{AB}$ is the Flory–Huggins parameter); hence the lamellar structure can be described by the so-called strong segregation limit theory[21] and the periodicity of the lamellar structure is given by (see Figure 1a,b):[21]

$$H = \frac{4}{6^{1/2}}\left(\frac{12}{\pi^2}\right)^{1/3} aN^{2/3}\chi^{1/6} \tag{2}$$

We assume that A and B blocks have preferential interactions with the air and the substrate, respectively. In this case, the equilibrium film thickness is given by

$$d_n = (n + 1/2)H \tag{3}$$

where n is an integer. The mean film thickness determined by the spin-coating process is assumed to be d.

C. Nucleation (Formation) Stage. In this section we consider the formation of the critical domains (their typical size and depth) and the ordinary defects (their density as a function of domain coverage area fraction Φ). After the spin-coating process the film thickness d is in general not equal to any of the equilibrium values $(n + 1/2)H$, that is to say $d \neq d_n$. This corresponds to either compressive or straining elastic deformations of the future layers (which appear during annealing). If $d = (n + 1/2)H + \epsilon$ $(0 < \epsilon < H/2)$, then the film is strained, and upon annealing it will shrink, giving rise to the formation of island structures. If, on the other hand $d = (n + 1/2)H - \epsilon$, then the film is compressed, and upon annealing it will swell, thereby forming hole structures.

1. Depth of the Layer with the Domain Structure. The microscopic structure of the domains (islands or holes) is related to that of a single dislocation defect inside the lamellar structure. This dislocation defect results in (i) the deformation (bending and compression) of the smectic layers and (ii) an increase in the contact area between the upper layer and air. In principle, this dislocation can be situated at any depth inside the film. To determine the exact depth of the dislocations appearing in the film during the formation stage, the free energy of such a dislocation should be evaluated, taking into account the two energy inputs described above. It is rather reasonable to assume that the dislocations are formed at a depth such that the linear edge dislocation energy is minimized. The calculations of the two contributions to the linear dislocation energy have been performed in the literature.[22,23] The general conclusion of these papers is the following. For thick enough films $(d \gg H)$ in rigid contact with the substrate, the extremal depth position d_{disl} strongly depends on the value of the interfacial tension air/A block, σ_{air}. For very low surface tensions

$$\frac{\sigma_{air}}{(KB)^{1/2}} \equiv \kappa < 1 \tag{4}$$

where K is the bending (splay) modulus and B is the compression modulus of the lamellar structure, the dislocation is attracted to the free surface of the film $(d_{disl} \to 0)$. However, if inequality (4) is not fulfilled and the opposite is true (i.e. $\kappa > 1$), then the equilibrium position of the dislocation is approximately in the middle of the film:[22]

$$d_{disl} \simeq d/(1 + \bar{\kappa}) \qquad \bar{\kappa} \equiv [(\kappa - 1)/(\kappa + 1)]^{2/3} \tag{5}$$

From the strong segregation theory it is known that for a diblock copolymer smectic K and B can be described as

$$K \sim fH^2 \quad \text{and} \quad B \sim f \tag{6}$$

where

$$f \sim T\chi^{1/3}N^{-2/3}a^{-3} \tag{7}$$

is the bulk free energy density of the lamellar system. Hence, $(KB)^{1/2} \simeq \sigma_{AB}$ where σ_{AB} is the interfacial tension acting at the interface between the A and B blocks, $\sigma_{AB} \sim T\chi_{AB}^{1/2}/a^2$.

In real polymer systems σ_{AB} is usually smaller than σ_{air}. Hence, the dislocations should be located in some inner layer of the film, at a depth d_{disl}. Still, if the film is thin enough, we can expect that the energy difference between this extremal layer and the neighboring layers is large; hence the domain structure appearing during the formation stage is really a *one-layer* structure. However, the possibility of mixed structures (the presence of dislocations in two or more neighboring layers) should not be excluded in the analysis of real experimental situations.

2. Critical Domain Size. The other unknown factor regarding the formation of dislocations is the critical size of the domains. If the size of a domain is lower than the critical size, the domain will not be stable, and fluctuations will force the domain to relax to a homogeneous stretched state of the film. Let us find this critical size, R_{cr}, as a function of the area fraction Φ occupied by the domains. The way to find the critical domain size of a new phase is known from the time of Zeldovich.[20]

In the initial homogeneous state the film has the thickness d, which is close to some equilibrium value d_n. We denote the stretch amplitude as ϵ:

$$\epsilon \equiv \min_n |d - (n + 1/2)H| \tag{8}$$

It is directly related to the area fraction Φ occupied by the domains after termination of the nucleation stage:

$$\Phi = \epsilon/H \tag{9}$$

Suppose that a domain of radius R is going to appear in some layer inside the film. This will lead to a stress relaxation on an area $\lambda^2 \simeq \pi R^2/\Phi$. On the other hand, an additional edge defect of length $\simeq 2\pi R$ will appear in the film. The free energy which is gained from the appearance of this domain is

$$\delta\mathcal{F} \simeq \frac{B}{2}\left(\frac{\epsilon}{d}\right)^2 \lambda^2 d - 2\pi R\gamma \tag{10}$$

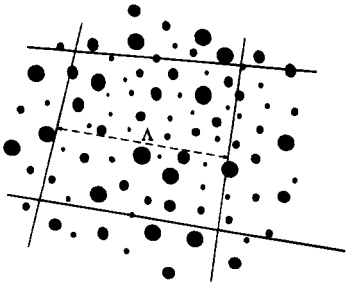

Figure 5. Top view of the surface showing typical defects with an average interdefect distance Λ.

where B is the compression modulus of the smectic phase (see eqs 6 and 7) and γ is the edge defect line tension:

$$\gamma \sim fH^2 \tag{11}$$

[In principle, the line tension γ can affect the height of the domains. It is easy to show that this effect is a small perturbation provided that the domain radius $R \gg H$. Therefore this effect can be neglected for the relief structure growth processes studied in this paper.] If $\delta\mathcal{F}(R) > 0$, the corresponding domain of size R will be stable. This is true for $R > R_{cr}$, where

$$R_{cr} \simeq \frac{4\gamma d}{BH^2\Phi} \sim \text{const} \times \frac{d}{\Phi} \tag{12}$$

is the so-called critical size of the domain (in eq 12 we have used eqs 6, 9, and 11).

Since the probability of a fluctuation leading to a domain of size R decreases exponentially with R, we can conclude that in the nucleation stage mostly domains of size R_{cr} will appear. So, the smaller the area fraction Φ occupied by domains, the larger is the typical size of the domains at the end of the nucleation stage of the spinodal decomposition process ($R_{cr} \propto \Phi^{-1}$, $\lambda_{cr} \propto \Phi^{-3/2}$). This conclusion is in agreement with experimental observations (see Figure 3b).

3. Density of Ordinary Defects. Simultaneously with the formation of the lamellar structure and the appearance of domains (circular dislocations), ordinary (linear) defects can also be formed in the regular layered structure of the film (see Figure 5). These linear defects are actually double edge dislocations; so they do not cause a long-range disturbance of the smectic structure. Neither an increase of the surface area of the film nor deformation of the layers (except the nearest ones) arises from such a pure defect (cf. Figure 4). Hence, the energy of a pure defect practically does not depend on its depth (cf. with section III.C.1). Therefore, these defects can emerge in all layers with equal probability.

However, if one considers defects in connection with the kinetics of relief structure domain growth, only the defects in the layer containing the domains and those in the neighboring ones will be important. To describe the density of such defects, we introduce a length parameter Λ, the mean interdefect distance (see Figure 5). The mean density of these defects is equal to $\rho_{def} \simeq \Lambda^{-1}$ (mean length of the defects per unit area).

The reason for the appearance of these defects is 2-fold. Either they can be formed as a result of stress relaxation processes in the film during the nucleation stage or the defects can appear due to various accidental factors. The former reason is the same as for the appearance of the domains; so we can expect that the corresponding input ρ_1 into the density of defects will be somehow connected with $\rho_{domains}$, the edge dislocation density in the domain structure at the end of the nucleation stage:

$$\rho_1 = \rho_1(\rho_{domains}) \qquad \rho_{domains} \simeq \left.\frac{2\pi R}{\lambda^2}\right|_{cr} \simeq \frac{2\Phi}{R_{cr}} \propto \Phi^2 \tag{13}$$

The latter input ρ_2 into the defect density is independent of Φ, because it is due to other, accidental reasons. Hence, the total density of defects ρ_{def} and the typical interdefect distance Λ are given by

$$\rho_{def} = \rho_1(\Phi) + \rho_2 \qquad \Lambda \simeq \rho_{def}^{-1} \tag{14}$$

Note that the position and density of defects are practically unchanged during the coalescence stage of the spinodal decomposition. Although the linear defects can relax toward a more straight shape to minimize their linear tension, they are very unlikely to diffuse as a whole because their corresponding characteristic diffusion time is very large (of order Λ^4; cf. eq 19 below). Hence, the defect density for the formation stage found in eq 14 also applies to the growth stage.

D. Coalescence (Growth) Stage. The main process during the coalescence stage of spinodal decomposition is the growth of the typical size of the domains. Both domain radius R and interdomain distance λ grow with time, while the area fraction covered by the domains remains constant:

$$\Phi \simeq \frac{\pi R^2}{\lambda^2} \simeq \text{const} \tag{15}$$

This leads to a decrease in the total length of the domain edge dislocations in the film ($\rho_{domains} \simeq 2\Phi/R$; see eq 13), and thus the total energy of the film is lowered. First we will look at such a growth process in an ideal film, i.e. a film without defects having all domains located in the same layer (see section III.D.1). After that we will study the possible consequences of the fact that the positions of the domains are not necessarily restricted to one unique layer (section III.D.2). Finally, we will discuss the role of defects in the domain growth process in section III.D.3.

1. One-Layer Domain Structure Relaxation in a Defectless (Ideal) Film. In the ideal case, all of the domains (islands or holes) are located in the same layer (see section III.C.1), and no defects (except for the domain edges) exist in the film (cf. section III.C.3). For this idealized situation we have proposed three main mechanisms of the growth process.[14] Below they will be considered in more detail and estimates for the characteristic time scales of each process will be calculated.

It is clear that the increase of the mean domain size R with time t can be either due to the fact that domains move as a whole or to collective relaxation flows of the block copolymer chains in the film. Hence, the following mechanisms for the domain size relaxation, which control the value of the critical exponent α ($R \propto t^{\alpha}$), should be considered:

(A) diffusional motion of the domains (inside the layer where they are located)

(B) two-dimensional pressure relaxation due to viscous flows inside coherent layers

(C) tunnel penetration of block copolymer chains into neighboring layers Below each mechanism will be

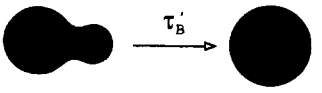

Figure 6. Relaxation of a noncircular domain toward a more circular shape. The characteristic time associated with this process is τ_B'.

considered separately and a complete picture of the processes involved in the coalescence stage (for an ideal film) will be presented.

(A) Diffusion of Domains. *Diffusional motion of the domains* is controlled by the friction coefficient between the neighboring layers in the block copolymer smectic phase. As a result, domains move, collide, and coalesce with each other. The characteristic time τ_A of this growth process can be found similarly as in classical Lifshitz–Slyozov calculations.[20] The two-dimensional analogue of the Lifshitz–Slyozov formula can be expressed as

$$\tau_A^{-1} \simeq cD \ln^{-1}(1/\Phi) \tag{16}$$

where c is the concentration of the domains

$$c \simeq \frac{\Phi}{\pi R^2} \tag{17}$$

and D is a characteristic coefficient of relative diffusion of typical domains in the film (at time t their size being $\sim R$):

$$D(R) \sim \frac{T}{\eta R^2} \qquad \eta \simeq \frac{\eta_{eff}}{H} \qquad \eta_{eff} \sim \frac{\zeta N^{4/9}}{a^2 \chi^{1/18}} \tag{18}$$

η_{eff} being the effective intralayer viscosity.[24] Hence, the characteristic time can be expressed as

$$\tau_A \sim \frac{\eta R^4 \ln(1/\Phi)}{\Phi T} \sim \left(\frac{\zeta}{a^2 T}\right) R^4 \left(\frac{\ln(1/\Phi)}{\Phi}\right) \frac{N^{4/9}}{\chi^{1/18}} \tag{19}$$

and so for this diffusional mechanism the critical exponent α is found to be

$$\alpha_A = 1/4 \tag{20}$$

(B) Two-Dimensional Flows. *Two-dimensional pressure relaxation* takes place inside coherent parts of the lamellar structure, e.g. inside islands or inside the matrix surrounding holes, or in continuous layers next to the layer containing the domain structure. If the curvature of the edge dislocation line is R, then the two-dimensional pressure in the layer matrix near this dislocation will be

$$\Pi = \gamma/R \tag{21}$$

Hence, in the vicinity of domains of different sizes, the pressures Π will be different, leading to a viscous flow. This flow, in turn, leads to an increase of larger domains at the expense of the smaller ones (the latter ones will gradually disappear). The characteristic time of this process is denoted as τ_B. If the shape of a domain is not circular, similar effects will lead to a smoothening of its border (see Figures 2 and 6). We denote the characteristic time for border smoothening as τ_B'.

In order to find characteristic times τ_B and τ_B' the following equations for viscous flows in a two-dimensional incompressible liquid should be solved:

$$\mathbf{v} = \frac{-\text{grad}\,\Pi}{\eta} \qquad \text{div}\,\mathbf{v} = 0 \tag{22}$$

If $\Phi \ll 1$, the typical interdomain distance $\lambda \gg R$ and the result for interdomain relaxation is as follows:[11]

$$\tau_B \sim \frac{\eta}{\gamma} R^3 \ln(\lambda/R) \sim \left(\frac{\zeta}{aT}\right) R^3 \ln(1/\Phi) \frac{1}{N^{2/9}\chi^{13/18}} \tag{23}$$

where the latter result is obtained using also eqs 11 and 18. In order to calculate the typical time for border smoothening τ_B' (like in Figure 6) we notice that the distance between the different parts of the same domain is of order R. Using eq 23, we get

$$\tau_B' \sim \tau_B|_{\lambda \sim R} \sim \frac{\eta}{\gamma} R^3 \sim \left(\frac{\zeta}{aT}\right) R^3 \frac{1}{N^{2/9}\chi^{13/18}} \tag{24}$$

and the critical exponent α for the B process is determined as

$$\alpha_B = {}^1/_3 \tag{25}$$

(C) Tunneling into Neighboring Layers. Suppose we have two islands of different sizes R_1 and R_2 in the same layer at a distance λ between them, and the diffusional motion of the islands (mechanism A according to our classification) is prohibited (e.g. the islands are very large). Then the only possible relaxation mechanism is *tunnel penetration of chains through the foreign layer* into a neighboring coherent layer where the relaxation via viscous flows (mechanism B) is possible (see Figure 7). If $R_1 < R_2$, then the pressure inside island "1" is higher (see eq 21), and chains would like to leave island "1" by penetrating into neighboring layers, which coherently connect both islands. Such relaxation includes two stages: the penetration through the foreign layers (near island "1" and near island "2"), which we will characterize by the time τ_C, and the two-dimensional pressure relaxation in the coherent layer (according to eq 22 characterized by the time τ_B). Therefore, the overall relaxation time for the mechanism of tunneling penetration will be the sum of the two characteristic times:

$$\tau_C^{full} = \tau_B + \tau_C \tag{26}$$

The probability p to find a block copolymer chain inside a foreign layer is very small, as it costs a considerable amount of energy. In order to estimate this energy F_b, the theory of Helfand[25] is used. The activation state here implies an almost completely stretched chain fragment inside the foreign layer (see Figure 8). This fragment includes m chain links, where m is given by

$$m \sim (3/8)^{1/2} H/(\chi^{1/2} a) \tag{27}$$

and its energy inside the foreign layer (measured from the level of the free energy inside its own layer far from the edge defects) can be expressed as

$$F_b \simeq \left(\frac{96}{\pi^2}\right)^{1/3} T(N\chi)^{2/3} \tag{28}$$

The probability p of finding a chain inside the foreign layer is directly related to this free energy barrier:

$$p \equiv \exp(-F_b/T) \tag{29}$$

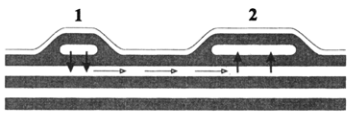

Figure 7. Schematic picture outlining the tunneling process (mechanism C; indicated by the thick arrows) and the two-dimensional relaxation process (mechanism B; indicated by thin arrows). Relaxation between the two islands (with radii R_1 and R_2) can take place by tunneling of polymer molecules followed by two-dimensional pressure relaxation.

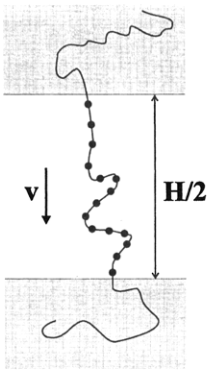

Figure 8. Schematic drawing of the tunneling process of a given block through the layer comprising the other block.

Consequently, among the chains present in a given island, there is a small fraction p which are in the process of penetration. The ratio of the number of links moving through the foreign layer and the total number of links in the island is pm/N. Therefore, the characteristic time of the tunnel penetration process $(\tau_C)_0$ is determined by the following formula:

$$(\tau_C^{-1})_0 \sim \frac{v}{H}\frac{m}{N}p \tag{30}$$

where v is the characteristic drift velocity of the chain links during the tunneling process. This velocity is governed by the difference between the chemical potentials inside the island and the layer into which the chains are penetrating, $\Delta\mu$:

$$v \simeq \frac{\Delta\mu}{\zeta H} \tag{31}$$

The chemical potentials are related to the corresponding osmotic pressures Π in the layers: $\Delta\mu \simeq \Delta\Pi a^3/H$. So the typical value of $\Delta\mu$ can be estimated (by using eq 21) as a function of the typical size of the islands:

$$\Delta\mu \sim \gamma a^3/(H\,R) \tag{32}$$

Thus, the final result for the characteristic time of the tunneling process is (using eqs 2, 7, 11, and 27−30)

$$(\tau_C)_0 \sim \left(\frac{\zeta a}{T}\right) RN^{5/3}\chi^{1/6}p^{-1}$$
$$p^{-1} \simeq \exp(2(12)^{1/3}\pi^{-2/3}T(N\chi)^{2/3}) \tag{33}$$

However, one can expect that the chains near the edge dislocation (near the boundary of the island) would penetrate into the foreign layers more readily. The reason for this is that the statistics of the chains near the dislocation is disturbed, and consequently their energy is higher than the energy of the chains in the middle of the island. Therefore, the corresponding tunneling barrier energy F_b' will be lower than the one for a typical chain located in the middle of an island, F_b:

$$F_b' \simeq F_b - \Delta F_b \qquad \Delta F_b \simeq m f a^3 \tag{34}$$

(see eqs 7 and 27). Analogous to the procedure above we can now determine the typical time $(\tau_C)_1$ for the tunneling of chains near the island borders. Since the fraction of chains near the boundary of an island is H/R, we find

$$((\tau_C)_1)^{-1} \simeq \frac{v}{H}\frac{m}{N}pp'\frac{H}{R} \qquad p' \simeq \exp(\Delta F_b/T) \tag{35}$$

We should of course take into account that the real characteristic time of the tunneling process is determined by both $(\tau_C)_0$ and $(\tau_C)_1$. So the final characteristic time τ_C is given by $\tau_C^{-1} = (\tau_C)_0^{-1} + (\tau_C)_1^{-1}$, resulting in

$$\tau_C \sim \left(\frac{\zeta a}{T}\right) RN^{5/3}\chi^{1/6}p^{-1}\left[1 + \frac{H}{R}p'\right]^{-1} \tag{36}$$

Consequently, the critical exponent α for the tunneling process can be either 1 (if $(\tau_C)_0 < (\tau_C)_1$) or $^1/_2$ (if $(\tau_C)_0 > (\tau_C)_1$).

For real block copolymer systems, estimations always give $p' \simeq 1$ ($\Delta F_b \sim T$; see eqs 2, 7, 27, and 34); hence the latter process (connected with $(\tau_C)_1$) is irrelevant for the relaxation of the domain structure. Thus for the characteristic time τ_C we can always use $(\tau_C)_0$ (see eq 33), and the critical exponent α for the C process is given by

$$\alpha_C = 1 \tag{37}$$

(D) Competition between the Three Main Mechanisms. Above we have described the process of domain size relaxation in an ideal defectless film, where all the domains are located in one and the same layer. We have come to the conclusion that the following values for the critical exponent α ($R \propto t^\alpha$) are possible: $^1/_4$, $^1/_3$, and 1 (see eqs 20, 25, and 37). Now we will describe a *complete* picture of the coalescence process in an *ideal* film and compare the characteristic times of the three processes described above (see eqs 19, 23, and 33).

Since the islands (holes) must be stable against temperature fluctuations, the inequality $\gamma R \gtrsim T$ should be fulfilled. So

$$\tau_B'/\tau_A \ll 1 \qquad \tau_B/\tau_A \ll 1 \tag{38}$$

(cf. eqs 19, 23, and 24). This is why the average shape of the domains is circular (see Figures 2 and 6). No matter how fast the diffusional motion of the islands, the relaxation to a circular shape must be even faster.

In the case of holes (in contrast to islands) each layer (with or without holes) is continuous, and thus process "C" is unimportant for this case. Hence, due to the inequality (38) the relaxation of hole structures in an ideal film is controlled merely by process "B" (flow relaxation), and the critical exponent in the case of hole structures should be $\alpha = ^1/_3$, according to eqs 23 and 25.

$$t_{\text{holes}}^{\text{ideal}} \simeq \tau_B \propto R^3 \tag{39}$$

In the case of island structures, the layer with the domains is discontinuous, and therefore the relaxation

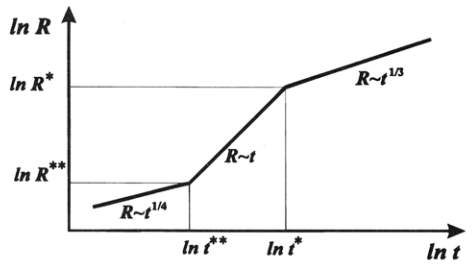

Figure 9. Time dependence of the relief structure size scale as a function of annealing time. Various regimes with different scaling behaviors are indicated in the graph.

via viscous flows is only possible through neighboring layers. The domain growth can proceed along two ways: either by diffusion of the islands (process "A") or by tunneling of chains from small islands into neighboring coherent layers, followed by hydrodynamic stress relaxation in these layers, and by tunneling of chains from these layers into bigger islands (combination of mechanisms "B" and "C"). Thus

$$t_{\text{islands}}^{\text{ideal}} \simeq \min\{\tau_A; \tau_C^{\text{full}}\} \simeq \min\{\tau_A; \tau_B + \tau_C\} \quad (40)$$

(see eqs 19, 23, and 33). The corresponding typical dependency of the characteristic island dimension versus time t is shown in Figure 9. The critical exponent α changes with time: $^1/_4 \rightarrow 1 \rightarrow {}^1/_3$. The characteristic scales for the crossover transitions between the regimes are given by

$$R^* \simeq a(p \ln(1/\Phi))^{-1/2} N^{17/18} \chi^{4/9}$$
$$R^{**} \simeq a\left(\frac{\Phi}{p \ln(1/\Phi)}\right)^{1/3} N^{11/27} \chi^{2/27} \quad (41)$$

One can estimate the values of the crossover scales R^* and R^{**} for any real block-copolymer system. For example, for the system used for the experiments described for the experiments described in section 2, this yields

$$R^{**} \sim 0.2\ \mu\text{m} \qquad R^* \sim 50\ \mu\text{m} \quad (42)$$

The following values have been used in eqs 33 and 41 in order to calculate the crossover scales R^{**} and R^*:

$$\chi \simeq 0.03 \qquad N \simeq 600 \qquad a \simeq 3\ \text{Å} \quad (43)$$

This means that the experimental situation is in the region $R^{**} < R < R^*$, where the apparent critical exponent α is equal to 1. However, the values R^* and R^{**} are very sensitive to the value of the Flory–Huggins parameter χ due to the exponential behavior of the factor p (see eqs 29 and 28). If a value of $\chi \simeq 0.1$ is used in eqs 33 and 41, the crossover values obtained are $R^{**} \sim 0.2$ mm and $R^* \sim 1$ m, and hence it should be concluded that the exponent $\alpha = {}^1/_4$. This is closer to experimental values (see Table 1), but still rather high, especially for the samples with small surface coverage.

To conclude the discussion of domain growth processes in defectless films, we have to mention that in the case of very thin films (in case the average thickness of the film is less than $H/2$; see Figure 10) the tunnel penetration process "C" is forbidden, as there are no neighboring layers in the film. Thus, for the case of island structures in such a very thin film the only

Figure 10. Typical island structures in case the average film thickness d is less than $H/2$. In this case, the tunnel penetration process is forbidden, the only relaxation mechanism available being the diffusional motion of islands.

relaxation process available is "A", and hence

$$t_{\text{islands}}^{\text{ideal}}(d < H/2) \simeq \tau_A \propto R^4 \quad (44)$$

2. Multilayered Domain Structures. In the previous subsection III.D.1 we have considered a pure situation, i.e. a defectless film containing domain structures located in one unique layer inside the film. In this ideal case the domain size growth is described by eqs 39, 40, and 44. This leads in all cases to values for the critical exponent α which are higher than the experimental ones (see Table 1). Also, theoretically, the behavior of hole structures (eq 39) should be very different from the island structures (see eqs 40 and 44). This is in disagreement with the experiments. One can expect that these discrepancies are connected with the fact that the experimental situation is not as ideal as considered previously in section III.D.1. Below we will discuss the possible consequences of various imperfections, starting with a situation in which the domain structures are not necessarily located in one and the same layer.

The existence of some optimum depth at which the energy of a domain edge dislocation is minimized has already been discussed in section III.C.1. Obviously, this depth may correspond to a level lying between a pair of neighboring lamellar layers in the film. It is therefore logical to expect that the domains might as well be located in both these neighboring layers. In principle, there is a non-zero probability for the appearance of domains even in layers other than these neighboring layers. Therefore, the domain structure of a *real* film formed upon annealing should be considered as being a *multilayered* domain structure.

(a) Domains Distributed in Several Layers. To understand the consequences of the fact that the domain pattern as observed in the experiments (e.g. Figure 2) is not a one-layer structure, but indeed a multilayered one, let us restrict ourselves to the case of a *two-layer* structure. Let us suppose that islands are present in two neighboring layers with surface coverages Φ_1 and Φ_2 ($\Phi_1 < \Phi_2$), and let the initial typical size of the islands in these layers (at the end of the nucleation stage) be of the same order: $R_1(t_0) \sim R_2(t_0)$. Depending on this size scale, the domain growth in each layer should evolve according to one of the three main mechanisms (see Figure 9 and eq 41). In accordance with eqs 19 and 23, the characteristic times of the "A" and "B" processes are Φ-dependent; i.e. the smaller Φ the slower the growth rate. E.g. for the process "A" (see eq 19)

$$\tau(R) \sim \text{const}\ R^4 f(\Phi) \quad (45)$$

where $f(\Phi) = \ln(1/\Phi)/\Phi$ decreases monotonically with Φ. For the case of a strongly asymmetric two-layer structure ($\Phi_1 \ll \Phi_2$) the typical time τ for a doubling of the domain size in these layers can differ strongly: e.g. for $\Phi_1 = 5\%$ and $\Phi_2 = 40\%$ in accordance with eq 45 $\tau_1/\tau_2 \simeq 26$, and for $\Phi_1 = 1\%$ and $\Phi_2 = 40\%$ $\tau_1/\tau_2 \simeq 200$. Hence, the domains in the layers with area fraction Φ_1

grow 26 (or 200) times slower than the domains in the layer with area fraction Φ_2.

The apparent mean area πR^2 of the domains in the film (domains inside both layers are now included) can be expressed as

$$\pi R^2 = \pi R_2^2 \frac{1 + \Phi_1/\Phi_2}{1 + (\Phi_1/\Phi_2)(R_2/R_1)^2} \tag{46}$$

where πR_1^2 and πR_2^2 are the number-averaged island areas in layers 1 and 2, respectively. If $\Phi_1 = 0$ then $R \propto t^{1/4}$ in accordance with eq 45. However, if $\Phi_1 \neq 0$, but $\Phi_1 \ll \Phi_2$, the apparent exponent α ($R \propto t^{\alpha}$) will be lower. At the beginning of the growth process the second term in the denominator in eq 46 can be neglected: $(\Phi_1/\Phi_2) \ll 1$; $(R_1/R_2) \sim 1$; remember that $R_1(t_0) \sim R_2(t_0)$. The initial increase of the mean area πR^2 is controlled mainly by the growth of πR_2^2:

$$\pi R^2 \simeq \pi R_2^2 \tag{47}$$

At later stages of the growth process ($t \to \infty$) the typical sizes of the domains in the layers i ($i = 1, 2$) will be

$$R_i(t) \simeq \text{const}[t/f(\Phi_i)]^{1/4} \tag{48}$$

(cf. eq 45). Hence, the apparent mean area of the islands will be

$$\pi R^2 = \pi R_2^2 \frac{1 + \Phi_1/\Phi_2}{1 + \left[\dfrac{\Phi_1 \ln(1/\Phi_1)}{\Phi_2 \ln(1/\Phi_2)}\right]^{1/2}} \qquad t \to \infty \tag{49}$$

which is lower than expected from eq 47. The crossover from eq 47 to eq 49 takes place at time scales of order τ_1 ($\tau_1 \gg \tau_2$), and it corresponds to an $(\tau_2/\tau_1)^{1/4}$ times increase in the scale of R_2.

For example for $\Phi_1 = 1\%$ and $\Phi_2 = 40\%$ the result of eq 49 is 25% less than the one of eq 47, and the crossover between eqs 47 and 49 corresponds to the time $\tau_1 \simeq 200\tau_2$, i.e. to a 14.1 times increase of the island area in the "main" layer πR_2^2 (or to a 10.6 times increase of the apparent area πR^2). Hence, for time scales of order τ_1, instead of the real critical exponent $\alpha = \ln R_2/\ln t = 0.25$ the experiment will give the value of the apparent exponent $\alpha_{app} = \ln R/\ln t \simeq 0.22$. For $\Phi_1 = 5\%$ and $\Phi_2 = 40\%$ similar considerations give $\alpha_{app}(\tau_1) \simeq 0.19$.

Hence, the hypothesis that the domains are distributed between two (or more) layers gives us a possible explanation for the reduced experimental values of the critical exponent α (see Table 1) as compared to the theoretical ones.

(b) Semi-Islands. As already mentioned above, the experimental behaviors of island and hole structures are rather similar (at least for finite time scales), although the theoretical consideration as presented in section III.D.1 gives different pictures for these types of structures (cf. eqs 39 and 40). One of the possible explanations is connected with the multilayer nature of the ensemble of domain structures.

Indeed, a detailed analysis shows that, assuming a multilayered domain structure, most of the islands must in fact be semi-islands (see Figure 11). That means that all of the layers inside the polymer film are continuous, even in the case of island structures. Hence, the domain growth proceeds via the flow relaxation mechanism ("B") for both islands and holes. Thus, for both cases the critical exponent α for relaxation *inside each layer* should be equal to $1/3$ (cf. with section III.D.1.D).

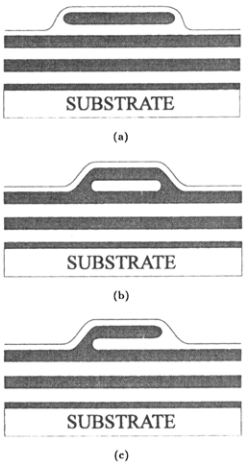

Figure 11. (a) Islands located in the top layer of the polymer film. (b) Islands located in the second white layer. (c) Structure of a semi-island: none of the layers is broken in this case.

If domain edge defects belong to *several layers*, the apparent exponent can be lower, as shown above (section III.D.2.A). For $\alpha = 1/3$, similar to section III.D.2.A, considerations show that the interference between several layers can lead to values $\alpha_{app} \simeq 0.25$. This is not enough, however, to explain the experimental values listed in Table 1. In the next subsection we will consider the possible imperfections in the film structure and discuss the so-called ordinary defects.

3. Role of Defects in the Domain Growth Process. As explained earlier in section III.C.3, during the nucleation stage of the spinodal decomposition, the appearance of domains is accompanied by the formation of ordinary (linear) defects. Some defects belong to the layers participating in the domain growth process, and hence they can slow it down. The density of such defects is described by eq 14. Below we will discuss the influence of these defects on the growth stage and on the value of the growth exponent α.

It is clear that at the end of the nucleation stage of the spinodal decomposition these defects are rather rare as compared to the density of domains:

$$\lambda_{cr} \lesssim \Lambda \tag{50}$$

If this were not the case, each domain would be cut into several ones by the defects. Thus at the beginning of the coalescence stage the situation is as shown in Figure 5. The linear defects cut the layers with domains into rather large districts, and the diffusional and flow relaxation mechanisms "A" and "B", respectively (see section III.D.1), are almost prohibited at spatial scales larger than Λ. In other words, relaxation across defects is possible only via tunneling processes (mechanism "C").

Hence, the growth process saturates at scales of order Λ. Indeed, if

$$\Lambda \lesssim \lambda^{**} \equiv (\pi/\Phi)^{1/2} R^{**} \tag{51}$$

(see section III.D.1.D and eq 41 for the definition of the scale R^{**}), the interdomain distance λ could (in the absence of defects) approach the value Λ before the crossover from regime "A" to regime "C" takes place (see Figure 9): $\tau_A(\Lambda) \lesssim t^{**}$ in accordance with eq 51 (see eqs 19 and 41). Therefore, at times corresponding to a

domain structure of scale Λ the process "C" is negligible compared with "A", and hence during the time $\tau_A(\Lambda) < t < t^{**}$ the interdomain distance λ is practically constant (in log-scale language): $\lambda \simeq \Lambda$, corresponding to the situation of one domain per $\Lambda \times \Lambda$ district. Such saturation of domain size growth for $\tau_A(\Lambda) < t < t^{**}$ leads to a strong decrease of the apparent critical exponent $\alpha_{app} \equiv \partial(\ln R)/\partial(\ln t)$ for times $t > t_A(\Lambda)$. If the experimentally accessible times are less than or on the order of t^{**}, the apparent exponent α_{app} will be significantly lower than the ideal value of $1/4$. Note, that at these times scales $\tau_A(\Lambda) < t < t^{**}$ the diffusional movement of the islands is already practically frozen (as the experimental time $t > \tau_A(\Lambda)$); however the islands still grow due to residual tunnel relaxation across the defect lines (via mechanism "C").

In case of hole or semi-island (see section III.D.2B) structures, when the ideal exponent is $\alpha = 1/3$, the condition where, at an interdomain scale $\lambda \sim \Lambda$, the defects can slow down the growth process (i.e. the condition where the tunneling process is weak compared with flow relaxation) is $\Lambda \lesssim R^*$ (cf. Figure 9). From the estimations of R^* performed in section III.D.1.D (see eq 42) it is clear that the experiments correspond to scales $\lambda \lesssim R^*$, and hence the defects really can keep $\lambda \sim \Lambda$ during the time available in experiments (i.e. between the time $\tau_B(\Lambda)$ and t^{**}).

Let us consider, for example, the experimental data shown in Figure 3. One can conclude that for the case of island structures the saturation takes place at $\lambda^2 \sim 30\ \mu m^2$, hence $\Lambda \gtrsim 5\ \mu m$. We suppose that the actual interdefect distance is $\Lambda \sim 10\ \mu m$. Note that in accordance with section III.C.2 the size of the critical domains increases with Φ (see eq 12), hence the smaller is Φ, the closer λ_{cr} is to Λ. Therefore, for small Φ the saturation will be more pronounced at the early stages of the growth process, and the apparent exponent α_{app} will be smaller. This prediction is in accordance with the experimental trend (see Table 1).

We can also conclude from the experimental data in section II that in our case the density of defects is practically independent of Φ (i.e. the input ρ_1 in eq 14 is small compared with ρ_2). However, in some other experiments (e.g. see Figures 5 and 6 from ref 8) the density of defects is Φ-dependent.

IV. Summary and Conclusions

We have considered both theoretically and experimentally the formation of relief structures (islands or holes) in block copolymer films. The coalescence stage during which the size of well-defined islands (or holes) increases with time was analyzed in detail. The main experimental result is the observation of the power law time dependence of the domain (island, hole) size with the apparent exponents, ranging from $\alpha = 0.12$ to 0.26, depending on the surface coverage Φ (the surface fraction of islands or holes). The lower Φ, the smaller is α. Any considerable difference between growth of islands and holes was not noticed. Our findings are in agreement with results reported earlier.[8]

In the Theoretical Part we have considered both the nucleation and the coalescence stage in the domain growth process. We have found that the typical domain size at the end of the nucleation stage is actually Φ-dependent: $R_{cr} \propto \Phi^{-1}$, and the relevant problems during the nucleation stage (the depth of domains, the formation of ordinary (linear) defects) were discussed.

The theoretical analysis of the coalescence stage (section III.D) consists of two parts. In section III.D.1, for an idealized situation (islands or holes in a single layer and no additional defects in the lamellar structure), the exponent α is predicted to be $1/4$, 1, or $1/3$ for islands (see Figure 9) and $1/3$ for holes. The parameters of the experimentally studied system fall into the region where the ideal exponent $\alpha = 1$ for islands. Thus the predictions are in marked disagreement with experimental observations.

In the second part (sections III.D.2–III.D.3) we tried to consider more realistic systems, abandoning the assumptions mentioned above. Namely, we took into account that (i) islands and holes can possibly appear not only on the top layer or inside a single internal layer but also simultaneously in several neighboring layers; (ii) more complex structures of elevations (like semi-islands; see Figure 11c) are possible; and (iii) line defects (like dislocations in ordinary crystals; see Figure 4) may be present in the system.

We have shown that all three factors give rise to a *decrease* of the apparent growth exponent α. In particular, the existence of a considerable amount of semi-islands can decrease the apparent growth exponent α from $\alpha = 1$ to $\alpha = 1/3$, and even to lower values if both islands and semi-islands are initially present.

The presence of line defects can give rise to a plateau in the domain size versus time dependence, thereby reducing α considerably. The effect of defects is most important for small values of the surface coverages Φ. These predictions are in qualitative agreement with the experimental results (both presented in this paper and reported earlier[8]). Submonolayer films, as investigated by Bassereau et al.[2] should diminish the influence of possible defects. They have observed an exponent of $\alpha = 0.23$ ($\Phi = 0.30$) which is in excellent agreement with our prediction (see eq 44). The important directions for future work are (1) to observe explicitly the defects and to analyze their distribution inside the film; (2) to measure the relative fraction of semi-islands and other complicated domains of unusual structure; (3) to analyze both theoretically and experimentally the dynamics of defect formation and to determine the main factors that control the density of defect lines; and (4) to observe the lamellar alignment at the domain edges as a function of the film thickness to determine the influence of possible homogeneous alignment of lamellae on the annealing behavior of the thin films.

Acknowledgment. We are grateful for the financial support of the Russian Foundation of Fundamental Research and the Dutch Foundation for Chemical Research (SON). We would also like to thank Dr. Rob v.d. Berg (Shell Research, Amsterdam) for his help during AFM image analysis.

References and Notes

(1) Bates, F. S. *Science* **1991**, *251*, 898.
(2) Bassereau, P.; Brodbreck, D.; Russell, T. P.; Brown, H. R.; Shull, K. R. *Phys. Rev. Lett.* **1993**, *71*, 1716. Coulon, G.; Daillant, J.; Collin, B.; Benattar, J. J.; Gallot, Y. *Macromolecules* **1993**, *26*, 1582. Coulon, G.; Ausserre, D.; Russell, T. P. *J. Phys. Fr.* **1990**, *51*, 777. Coulon, G.; Collin, B.; Ausserre, D.; Chatenay, D.; Russell, T. P. *J. Phys. Fr.* **1990**, *51*, 2801. Cai, Z.; Huang, K.; Montano, P. A.; Russell, T. P.; Bai, J. M.; Zajac, G. W. *J. Chem. Phys.* **1993**, *98*, 2376.
(3) Cai, Z.; Huang, K.; Montano, P. A.; Russell, T. P.; Bai, J. M.; Zajac, G. W. *J. Chem. Phys.* **1993**, *98*, 2376. Coulon, G.; Daillant, J.; Collin, B.; Benattar, J. J.; Gallot, Y. *Macromolecules* **1993**, *26*, 1582. Mayes, A. M.; Russell, T. P.; Bassereau, P.; Baker, S. M.; Smith, G. S. *Macrmolecules* **1994**, *27*, 749.
(4) Mayes, A. M.; Russell, T. P.; Bassereau, P.; Baker, S. M.; Smith, G. S. *Macromolecules* **1994**, *27*, 749. Menelle, A.;

Russell, T. P.; Anastasiadis, S. H.; Satija, S. K.; Majkrzak, C. F. *Phys. Rev. Lett.* **1992**, *68*, 67. Sikka, M.; Singh, N.; Karim, A.; Bates, F. S.; Satija, S. K.; Majkrzak, C. F. *Phys. Rev. Lett.* **1993**, *70*, 307. Russell, T. P.; Menelle, A.; Anastasiadis, S. H.; Satija, S. K.; Majkrzak, C. F. *Macromolecules* **1991**, *24*, 6263.

(5) Coulon, G.; Russell, T. P.; Deline, V. R.; Green, P. F. *Macromolecules* **1989**, *22*, 2581.

(6) Cai, Z.; Huang, K.; Montano, P. A.; Russell, T. P.; Bai, J. M.; Zajac, G. W. *J. Chem. Phys.* **1993**, *98*, 2376. Maaloum, M.; Ausserre, D.; Chatenay, D.; Coulon, G.; Gallot, Y. *Phys. Rev. Lett.* **1992**, *68*, 1575. Collin, B.; Chatenay, D.; Coulon, G.; Ausserre, D.; Gallot, Y. *Macromolecules* **1992**, *25*, 1621. Grim, P. C. M.; Psaros, M.; ten Brinke, G.; Hadziioannou, G. *Polym. Prepr. (Am. Chem. Soc., Div. Poly. Chem.)* **1994**, *35*, 125.

(7) Carvalho, B. L.; Thomas, E. L. *Phys. Rev. Lett.* **1994**, *73*, 3321.

(8) Coulon, G.; Collin, B.; Chatenay, D.; Gallot, Y. *J. Phys. II Fr.* **1993**, *3*, 697.

(9) Lifshitz, I. M.; Slyozov, V. V. *J. Phys. Chem. Solid* **1961**, *19*, 35.

(10) Fratzl, P.; Lebowitz, J. L.; Penrose, O.; Amar, J. *Phys. Rev. B* **1991**, *44*, 4794.

(11) Ausserré, D.; Chatenay, D.; Coulon, G.; Collin, B. *J. Phys. Fr.* **1990**, *51*, 2571.

(12) Binder, K. *Phys. Rev. B* **1977**, *15*, 4425.

(13) Mouritsen, O. G. In *Kinetics of Ordering and Growth at Surfaces*; Lagally, M., Ed.; NATO ASI Series B; Plenum: New York, 1990; Vol. 239.

(14) Nyrkova, I.; Semenov, A. N. *Polym. Prepr. (Am. Chem. Soc., Div. Polym. Chem.)* **1994**, *35*, 564.

(15) Grim, P. C. M.; Psaros, M.; ten Brinke, G.; Hadziioannou, G. *Polym. Prepr. (Am. Chem. Soc., Div. Polym. Chem.)* **1994**, *35*, 125.

(16) Tang, W. T. Dissertation, Stanford University, 1987, pp 139–141, 157.

(17) Binnig, G.; Quate, C. F.; Gerber, Ch. *Phys. Rev. Lett.* **1986**, *56*, 930.

(18) Frommer, J. *Angew. Chem., Intl. Ed. Engl.* **1992**, *31*, 1298.

(19) Maaloum, M.; Ausserre, D.; Chatenay, D.; Coulon, G.; Gallot, Y. *Phys. Rev. Lett.* **1992**, *68*, 1575.

(20) Landau, L. D.; Lifshitz, E. M. *Statistical Physics*, 3rd ed.; Pergamon Press: Oxford, U.K., 1980; Part 1.

(21) Semenov, A. N. *Sov. Phys. JETP* **1985**, *61*, 733.

(22) Lejcek, L.; Oswald, P. *J. Phys. II Fr.* **1991**, *1*, 931.

(23) Turner, M. S.; Maalloum, M.; Ausserré, D.; Joanny, J.-F.; Kunz, M. *J. Phys. II Fr.* **1994**, *4*, 689.

(24) Joanny, J.-F. *Langmuir* **1992**, *8*, 989.

(25) Helfand, E. *Macromolecules* **1992**, *25*, 492.

MA950303R